Int. J. Heat Mass Transfer. Vol. 18, pp. 1387–1396. Pergamon Press 1975. Printed in Great Britain

TOTAL AND LOCAL HEAT TRANSFER FROM A SMOOTH CIRCULAR CYLINDER IN CROSS-FLOW AT HIGH REYNOLDS NUMBER

ELMAR ACHENBACH
Kernforschungsanlage Jülich, Institut für Reaktorbauelemente,
517 Jülich, Postfach 1913, Germany

(*Received* 12 *June* 1974)

Abstract—The total and local heat transfer from a smooth circular cylinder to the cross flow of air has been measured over the Reynolds number range $3 \times 10^4 < Re < 4 \times 10^6$. The interaction between flow and heat transfer is discussed. In particular, the boundary-layer effects on the heat transfer, such as transition from laminar to turbulent flow or boundary-layer separation, are considered in conjunction with the distributions of local static pressure and skin friction.

NOMENCLATURE

b, width of the test section [m];
c_p, specific heat at constant pressure [Ws/kg K];
d, diameter of the test cylinder [m];
D, pressure drag [N];
f, vortex shedding frequency [1/s];
F, friction force [N];
k, coefficient, defined in the text;
l, length of the test cylinder [m];
m, number of periods of a cosine-function;
n, exponent of the Reynolds number;
p, pressure [N/m^2];
p_∞, pressure in the undisturbed flow [N/m^2];
q, heat flux [W/m^2];
r, radial coordinate [m];
R, outer radius of the test cylinder [m];
T, temperature [K];
ΔT, temperature variation at the surface of the test cylinder [K];
u', velocity fluctuation in flow direction [m/s];
U_∞, undisturbed velocity [m/s].

Greek symbols

α, heat-transfer coefficient [W/m^2 K];
δ_1, displacement thickness of the boundary layer [m];
ε, coefficient of radiation;
η, fluid viscosity [kg/(s m)];
ϑ, temperature difference wall-gas [K];
λ, heat conductivity [W/m K];
ρ, fluid density [kg/m^3];
τ_0, wall shear-stresses [N/m^2];
φ, circumferential angle, measured from the front stagnation point.

Characteristic numbers

B, $= d/b$, blockage ratio;
c_d, $= D/[(\rho/2)U_\infty^2 l.d]$, total drag coefficient;
c_f, $= F/[\rho/2)U_\infty^2 l.d]$, friction coefficient;
Nu, $= (\alpha d)/\lambda$, total Nusselt number;
Pr, $= \eta c_p/\lambda$, Prandtl number;
Re, $= U_\infty d\rho/\eta$, Reynolds number;
S, $= (fd)/U_\infty$, Strouhal number.

1. INTRODUCTION

IN THIS paper the heat transfer from a smooth circular cylinder in cross-flow is considered up to the Reynolds number of 4×10^6. Thus the range, where experimental data are already available, is exceeded by one order of magnitude. Schmidt and Wenner [1] achieved a maximum Reynolds number of $4{\cdot}25 \times 10^5$ in their test facility. Under conditions of normal temperature and pressure, such values can only be reached in air by using either big wind tunnels or high tunnel blockages, $B = d/b$, and small span ratios, $1/d$. The latter method was employed by Schmidt and Wenner who used values of $d/b = 0{\cdot}414$ and $1/d = 1$. Similar conditions also hold for Kroujilin's [2] tests whose heat-transfer results, however, seem to be too high compared with those of other authors. In the present investigations the difficulties associated with achieving high Reynolds numbers were overcome by using a high pressure wind tunnel. Since the Reynolds number, defined as $Re = U_\infty \rho d/\eta$, is proportional to the fluid density, it can be increased by increasing the static pressure within the circuit.

It is well known that for Reynolds numbers greater than about 10^5 a considerable change of the flow around the cylinder is observed. In this paper the effects of parameters which can influence this change, such as turbulence level or surface roughness, are eliminated by keeping them constant, as far as possible. Only the effect of the Reynolds number on the gradual change from a laminar to a turbulent boundary layer is considered.

Of course, the change in the flow causes a change in the heat-transfer behaviour. This interaction is discussed by describing both the heat transfer and the flow phenomena. Concerning the flow data reference is made to the author's previous papers as well as recent, still unpublished results.

2. EXPERIMENTAL APPARATUS AND MEASUREMENT TECHNIQUES

The tests were carried out in two wind tunnels which have the same internal dimensions. One of them operates under atmospheric conditions, the other can be pressurized up to 40 bars to produce high Reynolds numbers. In the former tunnel, the Reynolds number was varied over the range $3 \times 10^4 < Re < 3 \times 10^5$. The high pressure wind tunnel covered the range $1{\cdot}8 \times 10^5 < Re < 4 \times 10^6$, and thus the Reynolds numbers reached in the two tunnels overlapped. The fluid used was air at a temperature of about 30°C. Thus the results are presented only for a Prandtl number of 0·71. The turbulence level, Tu, defined by:

$$Tu = \frac{\sqrt{(\overline{u'^2})}}{U_\infty}$$

where u' corresponds to the velocity fluctuations in the flow direction and U_∞ to the velocity of the incident flow, had a value of about 0·45 per cent.

Figure 1 shows a sketch of the test section. The cylinder had a length, l, of 0·5 m and a diameter, d, of 0·1472 m. The cylinder was mounted in the rectangular test section which had a cross-section, $l \times b$, of $0{\cdot}5 \times 0{\cdot}9\,m^2$. Thus the blockage ratio was 0·164 and the span ratio 3·4. Details of the wind tunnel are described in [3].

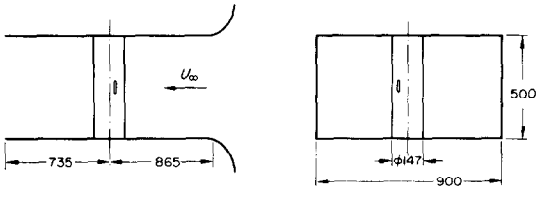

FIG. 1. Sketch of the test section.

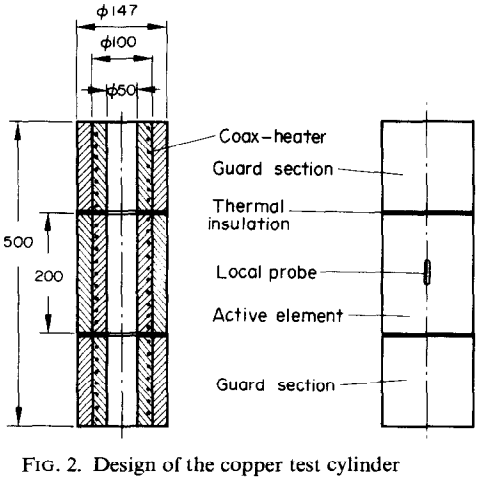

FIG. 2. Design of the copper test cylinder (scheme).

Figure 2 illustrates the copper test cylinder. It is divided into three parts. The centre piece is the active element for the measurement of the total heat-transfer rate; additionally, it supports the local heat-transfer probe. The active element is flanked by two guard sections, thermally insulated in order to eliminate wall

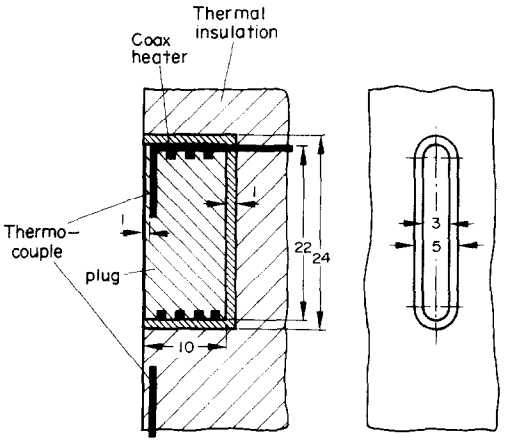

FIG. 3. Detail of the local heat-transfer probe.

effects. The three elements are separately heated from inside. Coaxial heaters are inserted into the copper rod and soldered with silver solder. Alternating current was passed through the heaters. The guard sections were held at the temperature of the active element to within ±0·1 K. The temperature difference between wall and gas varied from 5 to 75 K.

The local probe, which is schematically shown in Fig. 3, is a copper plug, thermally insulated from the surroundings and separately heated. The dimensions are: 3 mm wide, 22 mm long and 10 mm deep. The width subtends an angle of about 2·3° at the axis of the cylinder. The thermal insulation has a thickness of 1 mm. The plug was also held at the temperature of the cylinder within the same accuracy mentioned above. In all cases the temperature measurement was carried out by means of calibrated thermocouples.

The test cylinder could be rotated around its longitudinal axis in angular increments, $\Delta\varphi$, of 5°. Thus the local heat flux, as well as the local temperature distribution, could be measured.

The measured value of the electrical power, which was used for the determination of the total and local heat flux, has been corrected for losses in the electrical mains. In addition, the radiation rate was subtracted from the total rate, assuming the radiation coefficient, ε, to be 0·04 for highly polished copper surfaces.

For the determination of the local heat flux it was assumed that not only the surface of the plug, but also half the thickness of the thermal insulation should be considered as heat transferring area. However, for high Nusselt numbers it was expected that, because of the lower heat conductivity of the insulation material compared with copper, the temperature would decrease with increasing distance from the plug. This assumption was taken into account by a correction which had a maximum value of about 5 per cent for the highest Reynolds number.

To satisfy the boundary condition T_w = constant the test cylinder was made from copper, which has a high thermal conductivity (λ = 370 W/mK). Moreover, the walls were rather thick (25 mm) to compensate for the temperature differences caused by the non-uniform angular distribution of the heat-transfer coefficient. The

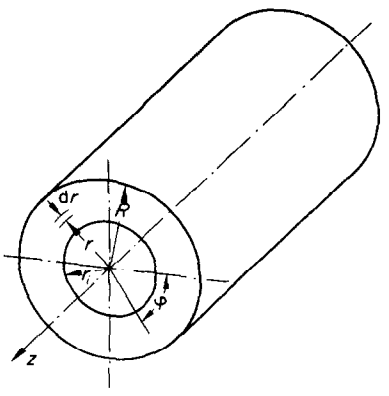

FIG. 4. Sketch of co-ordinate axes.

maximum deviation of the local temperature from the mean value was calculated from a rough approximation of distribution of heat-transfer coefficient around the circumference of the cylinder. The mathematical conditions were (for explanation of the symbols used, see Fig. 4):

1. Steady and two-dimensional flow (infinite cylinder)
2. For $r = r_i$: $q_{r(r_i,\varphi)} = \text{const}$, i.e. the radial heat flux at the inner radius r_i is constant
3. For $r = R$, the local radial heat flux is a multiple cosine-function around the mean flux, $\bar{q}$, according to

$$q_{r(R,\varphi)} = \bar{q}(1 + k\cos m\varphi) \tag{1}$$

where $k = (q_{\max} - q_{\min})/2\bar{q}$ and m is the number of periods.

Under these conditions the differential equation

$$\frac{\partial^2 T}{\partial r^2} + \frac{1}{r}\frac{\partial T}{\partial r} + \frac{1}{r^2}\frac{\partial^2 T}{\partial \varphi^2} = 0 \tag{2}$$

can be solved analytically [4]. With the Nusselt number of the cylinder defined as:

$$Nu = \frac{\alpha 2R}{\lambda_{\text{gas}}} = \frac{\alpha d}{\lambda_{\text{gas}}} \tag{3}$$

and the mean local temperature difference between wall (T_w) and gas (T_g) given by:

$$\vartheta = T_w - T_g \tag{4}$$

the temperature variation, ΔT, on the surface of the cylinder can be expressed as:

$$\frac{\Delta T}{\vartheta} = \frac{Nu}{2}\frac{\lambda_{\text{gas}}}{\lambda_{\text{metal}}}\frac{k}{m}\frac{\left(\frac{R}{r_i}\right)^{2m} + 1}{\left(\frac{R}{r_i}\right)^{2m} - 1}\cos m\varphi \tag{5}$$

λ_{gas} and λ_{metal} are the thermal conductivities of the gas and the test cylinder material, respectively. Equation (5) has extreme values for $\cos m\varphi = \pm 1$. Hence the maximum relative temperature variation becomes

$$\left(\frac{\Delta T}{\vartheta}\right)_{\max} = \pm\frac{Nu}{2}\frac{\lambda_{\text{gas}}}{\lambda_{\text{metal}}}\frac{k}{m}\left[\frac{\left(\frac{R}{r_i}\right)^{2m} + 1}{\left(\frac{R}{r_i}\right)^{2m} - 1}\right]. \tag{6}$$

The term in the square brackets in equation (6) denotes the geometrical influence of the radial heat flux on the temperature distribution. The factor becomes unity for $(R/r_i) \to \infty$, i.e. for a cylinder heated from the axis (thick walls).

As the relative temperature variation is proportional to the Nusselt number, the maximum value for $\Delta T/\vartheta$ is expected to occur when the maximum Nusselt number is reached. For the determination of the maximum temperature variation around the cylinder, the following data are introduced into equation (6)

$$Nu = 4300 \quad \text{at} \quad Re = 4 \times 10^6$$

$$\frac{\lambda_{\text{air}}}{\lambda_{\text{copper}}} = 7{\cdot}8 \times 10^{-5}$$

$$\left.\begin{aligned} k &= 0{\cdot}5 \\ m &= 2 \end{aligned}\right\} \text{from Fig. 9.}$$

Hence equation (6) yields:

$$\left(\frac{\Delta T}{\vartheta}\right)_{\max} = \pm 0{\cdot}064.$$

The experimental temperature distribution shown in Fig. 5 indicates a temperature variation around the cylinder of about ± 5 per cent. In view of the simplifications made, this is in good agreement with the value predicted.

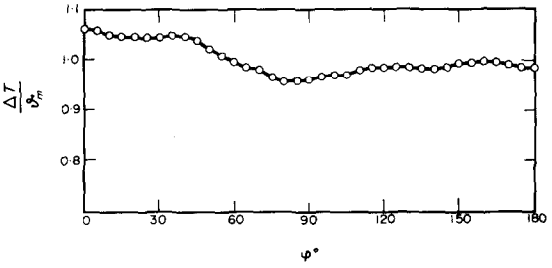

FIG. 5. Temperature distribution around the cylinder for $Re = 4 \times 10^6$ and $Pr = 0{\cdot}71$.

For the calculation of the total heat-transfer coefficient, the mean value, ϑ_m, of the temperature distribution around the circumference of the cylinder must be determined from equation (7):

$$\vartheta_m = \frac{1}{Nu 2\pi}\int_0^{2\pi} Nu_{(\varphi)}\vartheta_{(\varphi)}\,\mathrm{d}\varphi. \tag{7}$$

Equation (7) was evaluated numerically using the 72 experimental values of the local temperature and heat-transfer coefficient.

3. RESULTS

3.1. *Local flow and heat-transfer parameters*

In the Reynolds number range covered by the present investigation, the flow passes through four states: the subcritical, the critical, the supercritical and the transcritical regime. Each of the flow states is represented below by a diagram which contains the distributions of the local static pressure, local skin friction and local heat-transfer coefficients. From these diagrams the characteristics of each of the flow regimes become evident.

The results are presented in a dimensionless form. The following definitions are used

$$\text{static pressure:}\quad \frac{p-p_\infty}{\frac{\rho}{2}U_\infty^2}$$

$$\text{skin friction:}\quad \frac{\tau_0}{\rho U_\infty^2}\sqrt{(Re)}$$

$$\text{heat transfer:}\quad \frac{Nu}{\sqrt{(Re)}}.$$

The static pressure, as well as the skin friction, are made dimensionless by the dynamic pressure of the incident flow. Furthermore, the skin friction and the heat-transfer coefficient are normalized by the square root of the Reynolds number. The local Nusselt number is formed using the tube diameter as the length scale together with the local heat-transfer coefficient $\alpha = \alpha_{(\varphi)}$.

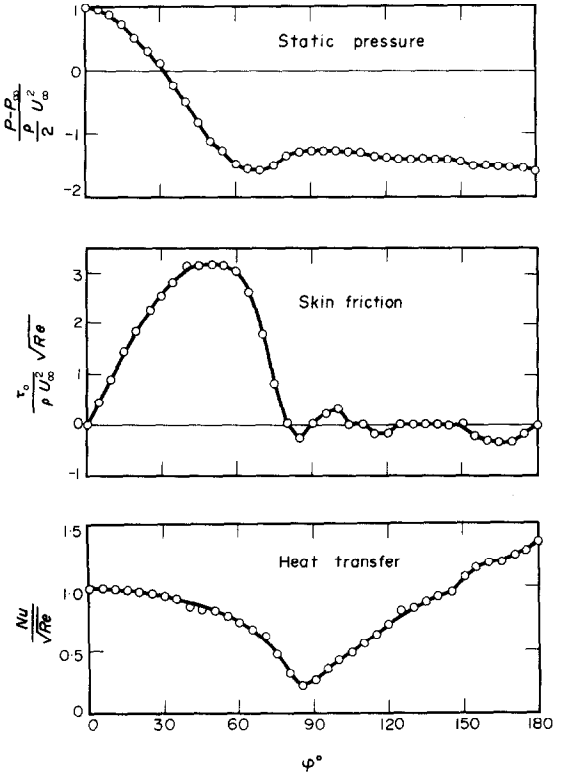

FIG. 6. Subcritical flow: local distributions of static pressure, skin friction and heat transfer around the cylinder, $Re = 10^5$, $Pr = 0{\cdot}71$.

The subcritical flow is dealt with in Fig. 6 for $Re = 10^5$. The static pressure drops with increasing distance from the stagnation point. The pressure forces accelerate the flow so that the wall shear-stresses rapidly increase. At the same time the local heat-transfer coefficient gradually diminishes, starting at $\varphi = 0$ with the value calculated for the stagnation point, i.e. $Nu/\sqrt{(Re)} = 1{\cdot}01$ [5].

With increasing distance from the stagnation point the experimental static pressure distribution deviates more and more from the distribution provided by potential theory. At $\varphi = 70°$, the pressure minimum has already been reached, $(p-p_\infty)/[(\rho/2)]U_\infty^2$ having a value of only $-1{\cdot}6$ compared with -3 from the theory.

The wall shear stresses have a maximum at about $\varphi = 50°$. Downstream of the position $\varphi = 60°$ they drop rapidly, since the pressure gradient approaches zero. Finally, the wall shear-stresses vanish. The boundary layer is no longer able to move against the positive pressure gradient. It laminarly separates from the front part of the cylinder at about $\varphi = 80°$; some degrees downstream, the heat transfer passes a minimum value as a consequence of vanishing skin friction. Downstream of the separation point, the static pressure slowly decreases from $-1{\cdot}3$ to $-1{\cdot}6$. The temporal mean value of the skin friction moves around zero

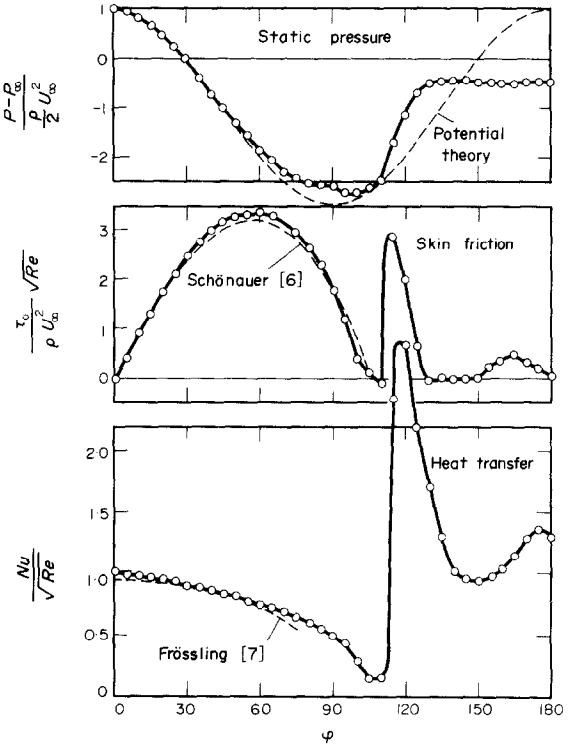

FIG. 7. Critical flow: local distribution of static pressure, skin friction and heat transfer around the cylinder. $Re = 4 \times 10^5$, $Pr = 0{\cdot}71$. ---- Theory after Schönauer [6] and Frössling [7], respectively.

and indicates that there is no boundary layer established. Downstream of the separation point, the heat-transfer coefficient continuously increases up to values which lie about 30 per cent above those of the stagnation point. The improved heat transfer in the rear of the cylinder is due to the increased transverse exchange of fluid in the separated flow region.

The critical flow range is represented by Fig. 7. The Reynolds number is $Re = 4 \times 10^5$. Over a large distance from the stagnation point the experimental static pressure distribution is nearly identical with the theoretical one. Up to $\varphi = 110°$ the maximum deviation is always smaller than 10 per cent. From this evidence it can be concluded that there will also be a good agreement between the experimental and theoretical results for the skin friction distribution. Figure 7

illustrates that this is, indeed, the case. There is an intermediate separation of the laminar boundary layer from the wall at about $\varphi = 107°$ (Schönauer [6] computed a value of $\varphi_s = 104{\cdot}45°$). Downstream a separation bubble forms. The free shear layer becomes turbulent and reattaches to the wall with an intensive rise of the skin friction. The final separation occurs, in the present example, at about $\varphi_s = 130°$. The shift of the separation point far downstream causes the static pressure coefficient to increase to a value of $-0{\cdot}5$, which leads to a low drag coefficient.

The local heat-transfer coefficient continuously decreases, starting at $\varphi = 0$ with $Nu/\sqrt{(Re)} \approx 1$, until the intermediate separation occurs. The dashed line represents the theoretical result predicted by Frössling [7]. The minimum near the separation bubble is succeeded by an enormous improvement of the heat transfer because of the increased exchange of fluid normal to the wall due to onset of turbulence. The heat-transfer coefficient reaches a value three times higher than at the front stagnation point. Further downstream the wall shear stresses rapidly decrease and cause a reduction of the heat transfer. At $\varphi = 150°$, a relative minimum is observed which is succeeded by a small increase of the heat transfer. It is remarkable that, in the separated flow region, the dimensionless heat-transfer coefficient is equal to that of the subcritical case.

The supercritical flow is described by means of Fig. 8 for $Re = 1{\cdot}27 \times 10^6$. This flow regime is distinguished from the critical one by the fact that no intermediate separation occurs. A direct transition from the laminar to the turbulent boundary layer is observed downstream of the main cross-section. The separation point moves some degrees towards the front stagnation point and causes a lower base pressure than for critical conditions. As far as the local heat-transfer distribution is concerned, no clear differentiation is possible between critical and supercritical flow state. The only small difference to be noticed is that the minimum value of heat transfer near the transition point is somewhat higher than for the critical flow, since the wall shear stresses do not vanish.

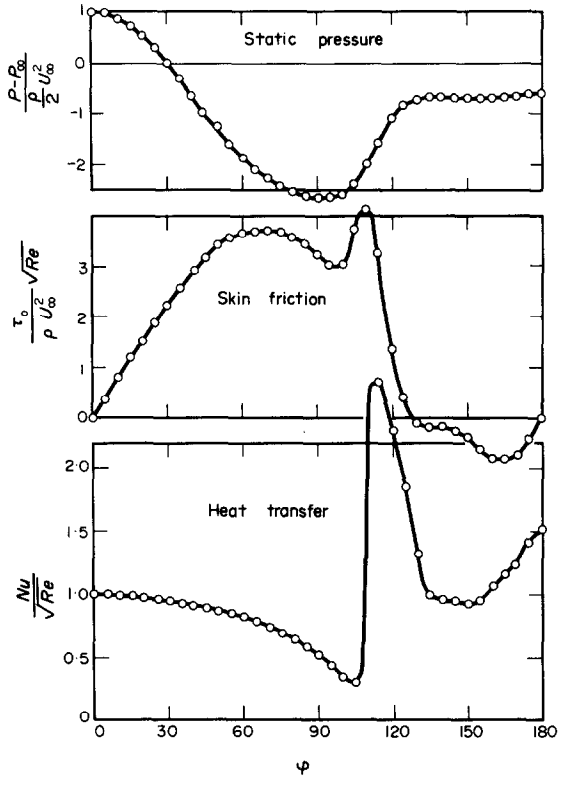

FIG. 8. Supercritical flow: local distribution of static pressure, skin friction and heat transfer around the cylinder. $Re = 1{\cdot}27 \times 10^6$, $Pr = 0{\cdot}71$.

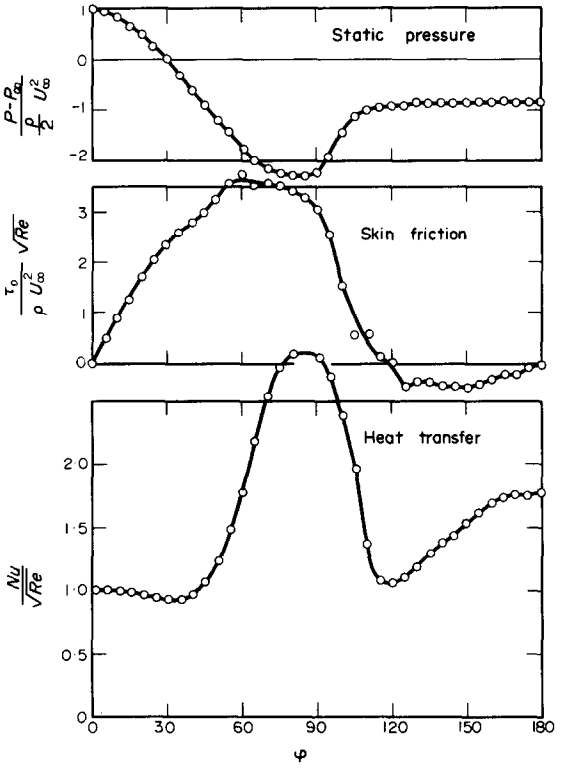

FIG. 9. Transcritical flow: local distribution of static pressure, skin friction and heat transfer around the cylinder, $Re = 4 \times 10^6$, $Pr = 0{\cdot}71$.

Figure 9 illustrates the results for the transcritical flow at $Re = 4 \times 10^6$. The distribution of the skin friction, as well as of the heat-transfer coefficient, indicate that the boundary layer changes from laminar to turbulent flow right at the front of the cylinder at $\varphi_t = 35°$. With further increase of the distance from the stagnation point, the local heat transfer increases and reaches its maximum at $\varphi = 85°$, having a value three times that at the stagnation point. The heat-transfer coefficient then drops, corresponding to the decreasing wall shear stresses. Near the position of the separation point of the boundary layer, i.e. at $\varphi_s = 120°$, the heat-transfer coefficient has a relative minimum and finally, at the rear stagnation point, reaches a value of $Nu/\sqrt{(Re)} = 1{\cdot}75$.

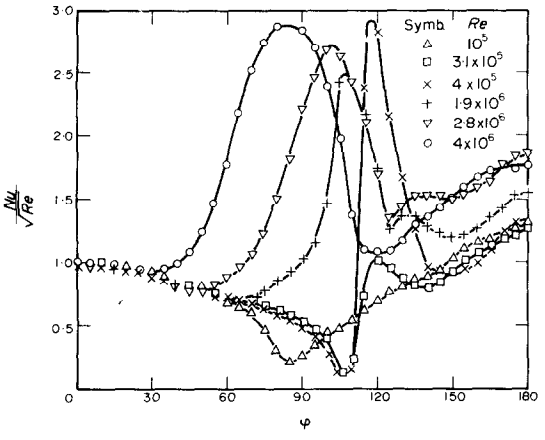

FIG. 10. Effect of Reynolds number on the local heat-transfer distribution around a cylinder, $Pr = 0{\cdot}71$.

The effect of the Reynolds number on the local heat-transfer distribution is summarized in Fig. 10. The shift of the point of boundary-layer separation as well as that of the boundary-layer transition, both discussed in the context of Fig. 14, become evident.

In the critical flow range two experimental curves are presented; these demonstrate how the peak due to the turbulently reattached boundary layer grows with increasing Reynolds number. Near the critical Reynolds number, $Re = 3{\cdot}1 \times 10^5$, the turbulent boundary layer seems to be not yet fully developed, as it is for instance at $Re = 4 \times 10^5$. Furthermore, it is remarkable that, over the entire critical flow regime, the dimensionless heat transfer around the rear stagnation point is nearly as low as for the subcritical Reynolds number $Re = 10^5$.

For $Re = 1{\cdot}9 \times 10^6$ the transition from laminar to turbulent boundary layer already occurs on the front part of the cylinder at $\varphi_t = 70°$, which means that the transcritical flow state will be established. The rearward heat transfer increases with a power of the Reynolds number greater than 0·5. The heat-transfer distributions for $Re = 2{\cdot}8 \times 10^6$ and $Re = 4 \times 10^6$ again show the rapid shift of the transition point to the front stagnation point with increasing Reynolds number.

The evaluation of the experimental local heat-transfer distributions permits a discretization of the particular contributions of heat transfer through regions of laminar boundary layer, separated flow and turbulent boundary layer. In Fig. 11, the corresponding demarcation lines are drawn. For subcritical conditions

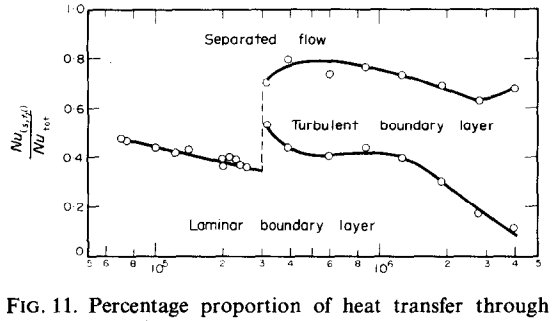

FIG. 11. Percentage proportion of heat transfer through laminar boundary layer, turbulent boundary layer and separated flow.

the flow around the cylinder is either laminar or separated. The percentage contribution of the heat transfer through the laminar boundary layer decreases from about 47 per cent at $Re = 7 \times 10^4$ to 35 per cent at $Re = 3 \times 10^5$. Beyond the critical Reynolds number there exists an additional region characterized by a turbulent boundary layer. The turbulent contribution lies between 35 and 40 per cent in the Reynolds number range $4 \times 10^5 < Re < 2 \times 10^6$. Of course, this percentage will increase in the transcritical flow range, since the area of the cylinder that is covered with a turbulent boundary layer becomes more extensive with increasing Reynolds number. At $Re = 4 \times 10^6$ the contribution is about 60 per cent. The increasing trend is, above all, to the detriment of the contribution from heat transfer through the laminar portion of the boundary layer. This proportion is only 10 per cent for $Re = 4 \times 10^6$.

Near the critical Reynolds number the contribution from the separated region of the cylinder to the total heat transfer drastically drops from 65 down to about 20 per cent. This amount gradually increases with increasing Reynolds number and shows, for the highest Reynolds number reached, a value of about 30 per cent. It is surprising to see that, beyond the critical Reynolds number, 70–80 per cent of the total heat is transferred through a boundary layer flow. From this evidence it can be concluded that an important improvement of the heat transfer from the cylinder can be obtained by the well-known methods which influence the boundary-layer flow, such as surface roughening, for instance.

3.2. *Total heat transfer*

Figure 12 represents the experimental relationship between the total heat-transfer rate, Nu and the Reynolds number, over the range $3 \times 10^4 < Re < 4 \times 10^6$. The Prandtl number, Pr, is that of air at a temperature of about 305 K, i.e. $Pr = 0{\cdot}71$. The effect of the flow parameters on the experimental results is discussed, taking Fig. 14 into consideration. It is surprising that in spite of such important changes of the flow beyond $Re = 10^5$, as demonstrated in the preceding paragraph, the curve Nu vs Re is fairly smooth, apart from a deviation of -10 per cent in the critical flow

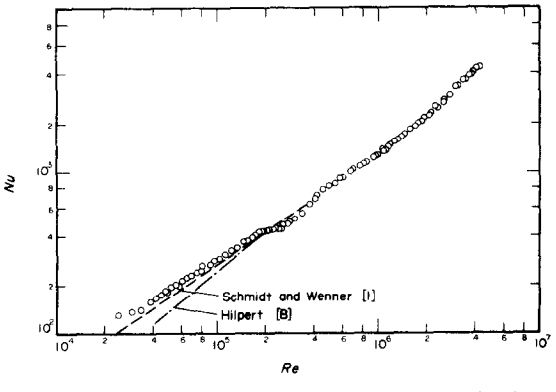

FIG. 12. Total Nusselt number of the smooth circular cylinder in cross flow as a function of Reynolds number, $Pr = 0{\cdot}71$.

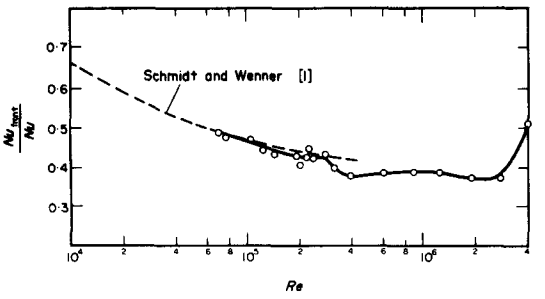

FIG. 13. Contribution of the frontal heat transfer to the total heat transfer from a cylinder, $Pr = 0{\cdot}71$.

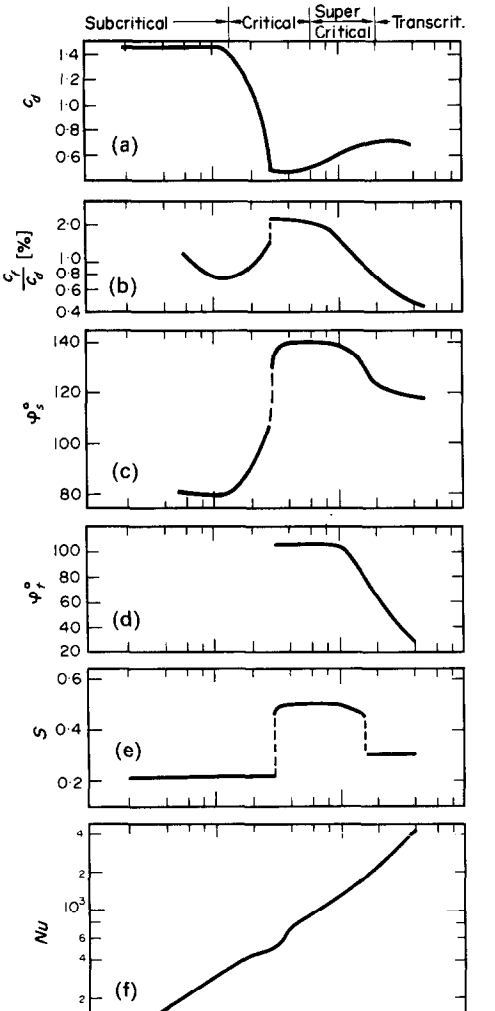

FIG. 14. Flow and heat-transfer parameters as a function of Reynolds number, $Pr = 0{\cdot}71$; (a) drag coefficient; (b) percentage contribution of friction to the total drag; (c) angle of boundary layer separation; (d) angle of boundary layer transition; (e) Strouhal number; (f) Nusselt number; (g) contribution of the frontal heat transfer to the total heat transfer.

regime. The same trend holds for the ratio of frontal heat transfer to total heat transfer as a function of the Reynolds number; this is shown in Fig. 13. Here an important effect occurs only in the transcritical flow range, where the frontal heat transfer is considerably improved due to the presence of a turbulent boundary layer.

A comparison between the data already available in the literature and the present results is possible only for subcritical flow conditions ($Re \leqslant 4 \times 10^5$). In Fig. 12, the results of Schmidt and Wenner [1], indicated by the dashed line, and the experimental data of Hilpert [8] are given. Both curves show a different slope from one another. They are steeper than the curve suggested by the present results, probably due to the effects of blockage and low span ratio mentioned earlier. Whereas Schmidt and Wenner's results provide reasonable agreement with the present data, Hilpert's curve deviates substantially, particularly at low Reynolds numbers.

Figure 13 illustrates the relationship between the ratio of frontal to total heat transfer and Reynolds number; the results of Schmidt and Wenner [1] are also presented in this figure. It is seen that their results agree well with the present ones, except near the critical Reynolds number.

Figure 14 is a combination of seven diagrams, which present some instructive flow and heat-transfer parameters as a function of the Reynolds number. The flow parameters are taken from a previous work and are as follows: drag coefficient c_d, skin friction as a percentage of the total drag, c_f/c_d [9], angular position of boundary-layer transition (laminar-turbulent), φ_t, vortex shedding frequency, f_d/U_∞ [10], average heat-transfer coefficient, Nu, and the ratio of frontal heat-transfer rate to the total value, Nu_{front}/Nu. This presentation demonstrates very clearly the interaction between the flow and heat transfer parameters.

At subcritical flow conditions the boundary layer separates laminarly at about $\varphi = 80°$ over a large range of the Reynolds number. The wake width as well as the dimensionless base pressure remain constant. Therefore the drag coefficient as well as the Strouhal number are independent of Reynolds number. At the same time the contribution of friction to the total drag diminishes by $Re^{-0{\cdot}5}$, as the boundary layer is laminar. The average heat-transfer coefficient increases with a slope of 0·63 which is greater than the "laminar slope" of 0·5. This effect is due to the increase of the rearward heat transfer with increasing Reynolds number. This trend is obvious on consideration of the decreasing value of Nu_{front}/Nu with increasing Reynolds number.

When $Re = 1{\cdot}2 \times 10^5$ is exceeded the separation point shifts downstream. This phenomenon must be seen in connexion with both the decrease of the displacement thickness δ_1 with $Re^{-0{\cdot}5}$ [11] and with the decrease of friction force as a percentage of the total drag. The latter effect means that proportionately less of the energy of the boundary layer is dissipated by friction forces with increasing Reynolds number. The reduction of the displacement thickness affects the static

pressure distribution, since the flow is able to follow the contour of the wall for a longer distance. This means, that the real pressure distribution gradually approaches the theoretical one, which has a negative pressure gradient for the whole front part of the cylinder. Both effects re-inforce one another so that the shift from $\varphi = 80$ to $\varphi = 90°$ occurs over a short range of Reynolds number, as is seen from the experiments. Finally, laminar boundary-layer separation occurs due to the positive pressure gradient. In fact the downstream shift of the laminar boundary-layer separation is observed over the Reynolds number range $1{\cdot}2 \times 10^5 < Re < 3 \times 10^5$, where φ_s changes from $\varphi_s = 80°$ to $\varphi_s = 110°$. Due to this change the base pressure increases and causes a considerable drop of the drag coefficient. This flow range which is called the critical one is quite sensitive to any disturbances of the flow. Any slight asymmetry or small obstacle on the surface would cause the boundary layer to change from laminar to turbulent flow, followed by a drastic change in the drag coefficient. The skin friction, as a proportion of the total drag, to the same extent as the total drag decreases. At the critical Reynolds number the Strouhal number rapidly changes from 0·21 to 0·5. This increase was expected, since the wake width diminishes in the critical flow range [12]. At about $Re = 1{\cdot}5 \times 10^6$ the wake width increases again associated with a decrease of the Strouhal number. In the transcritical flow regime shedding frequencies as known from Roshko were measured.

At $Re = 3 \times 10^5$ the critical Reynolds number is reached; it can be characterized by the Reynolds number corresponding to the minimum drag coefficient. Here the phenomenon of the separation bubble occurs, which has been described in connection with Fig. 7. At about $\varphi = 105°$ the boundary layer separates laminarly. The transition from the laminar to the turbulent free shear layer takes place. At $\varphi = 110°$ the shear layer reattaches to the wall as a turbulent boundary layer and finally separates at about $\varphi_s = 140°$. This flow state is observed up to $Re \approx 6 \times 10^5$. Since it is sensitive to disturbances, in a similar way to the flow state immediately before the critical Reynolds number, it is also assigned to the critical flow range. Whereas all flow parameters are distinguished in the critical flow regime, by considerable changes of the magnitude of their value with Reynolds number, the total heat-transfer behaviour is hardly affected. Both the ratio Nu_{front}/Nu and the total heat-transfer coefficient Nu vary by only 10 per cent. In the Reynolds number range $2 \times 10^5 < Re < 3 \times 10^5$, Nu remains nearly constant, due to the augmentation of the region covered by a laminar boundary layer where the heat transfer is low. For $Re > 3 \times 10^5$ Nu increases again; this is caused by the improvement of the heat transfer in rear of the cylinder, brought about by the transition to a turbulent boundary layer. This phenomenon also becomes evident on consideration of the ratio Nu_{front}/Nu as a function of the Reynolds number.

The supercritical flow regime extends from $Re \approx 6 \times 10^5$ to $Re \approx 2 \times 10^6$. It is characterized by an immediate transition from a laminar to a turbulent boundary layer downstream of the main cross section, i.e. for $\varphi > 90°$. The angle of boundary-layer separation reduces from $\varphi_s = 140$ to $\varphi_s \approx 120$ causing an increase in the drag coefficient. At the same time the contribution of the friction forces to the total drag decreases. The existence of the two frequency modes no longer occurs and Strouhal numbers were measured which were somewhat higher than those for the subcritical case, but with a larger scatter of the experimental results. The slope of the curve Nu vs Re gradually changes from 0·63 to 0·94 whereas the ration Nu_{front}/Nu remains nearly constant.

Once the transition from laminar to turbulent boundary layer occurs on the front part of the cylinder, it rapidly shifts towards the front stagnation point with increasing Reynolds number, whilst the position of the separation point remains nearly fixed. This evidence indicates the beginning of the transcritical flow regime where the drag coefficient as well as the Strouhal number reach a new plateau. In the present experiments the fully developed transcritical flow characterized by a nearly complete turbulent boundary layer is not yet reached entirely. Nevertheless, the trend is visible. With regard to the relationship between Nu and Re (Fig. 12), the experimental results around $Re = 4 \times 10^6$ indicate that the slope of the curve is going to reduce from 0·93 to a value which will probably be 0·8, corresponding to the heat transfer through turbulent boundary layers.

On the basis of experiments on the heat transfer from rough cylinders [13] it is expected that, for the fully developed transcritical flow, the ratio of frontal heat transfer to the total value lies between 0·60 and 0·65.

FINAL REMARKS

In the present paper the interaction between flow parameters and heat transfer was demonstrated. The techniques of measuring the static pressure and skin friction are not described here, but detailed information on these methods can be obtained from a previous paper devoted to the study of these parameters [9]. It should be noted that the local heat-transfer distribution was not determined in the same run as the local static pressure and the skin friction. In addition, two different test cylinders had to be used in order to accommodate the different instrumentation. Thus, the occurrence of small differences in the flow conditions between the various tests cannot be ruled out.

It has already been mentioned that the width of the local heat-transfer probe was 3×10^{-3} m which subtended an angle of about $\Delta\varphi = 2{\cdot}3°$ at the axis of the cylinder. The "finite" width of the probe as well as the conduction of heat in a circumferential direction falsify the true experimental curve, in the sense that sharp peaks tend to be levelled. This effect should be kept in mind whenever the curves show a steep increase, as, for instance, for the critical flow regime in the region $100° < \varphi < 150°$.

The tunnel blockage $d/b = 0{\cdot}164$ was even high and must have had some effect on the oncoming velocity

and hence on the drag coefficient, c_d. In spite of this rather high value no corrections for tunnel blockage was applied, as the equations given by Allen and Vincenti [14] do not hold for flow states where the drag coefficient varies considerably with Reynolds number. Some recent investigations by the author into the drag coefficient of a cylinder in cross-flow provided a relationship between c_d and Re. These tests were carried out using a cylinder without a skin friction probe which was thought in earlier experiments [9] to cause premature boundary-layer transition. Compared with [9] the present results show an effect of about 10 per cent in the range beyond the critical Reynolds number.

The effect of surface roughness was eliminated as far as possible by polishing the surface of the cylinder. However, the surface of the thermal insulation both separating the three individual parts of the test cylinder from one another and surrounding the local heat-transfer probe, could not be rendered as smooth as the remaining copper surface of the cylinder. This deficiency might locally cause premature transition effects, especially at very high Reynolds numbers. However, discrepancies between the heat transfer and the flow tests could not be observed.

The effect of the Prandtl number has not been considered since the results reported herein are valid for $Pr = 0{\cdot}71$ only, i.e. for gases. For this reason the author did not propose a correlation with respect to the exponent of the Prandtl number, but leaves this decision to the reader.

The heat-transfer tests may be regarded as having been conducted under quasi-isothermal conditions, because generally the temperature differences chosen were $\vartheta = 20\,\mathrm{K}$ or smaller. The properties of the fluid have been related to the temperature of the undisturbed gas flow.

Acknowledgements—These tests were carried out in connexion with investigations on the flow and heat transfer from heat exchangers in the laboratories of the "Institut für Reaktorbauelemente der Kernforschungsanlage Jülich". The author is grateful to the director of the Institute, Dr. C. B. von der Decken, who supported this work with great interest. The author also wishes to thank his assistants H. Gillessen, F. Hoffmanns, H. Reger and R. Rommerskirchen for their valuable help during the preparation and performance of the experiments.

REFERENCES

1. E. Schmidt and K. Wenner, Wärmeabgabe über den Umfang eines angeblasenen geheizten Zylinders, *Forsch. Geb. IngWes.* **12**(2), 65–73 (1941).
2. G. Kroujilin, The heat transfer of a circular cylinder in a transverse air flow in the range of $Re = 6000$–$425\,000$, *Tech. Phys. USSR* **5**(4), 289–297 (1938).
3. H. Grosse and F. Scholz, Der Hochdruck-Gaskanal, *Kerntechnik* **7**(4), 150–158 (1965).
4. H. S. Carslaw and J. C. Jaeger, *Conduction of Heat in Solids*, 2nd edn, pp. 188–193. Clarendon Press, Oxford (1959).
6. W. Schönauer, Ein Differenzenverfahren zur Lösung der Grenzschichtgleichung für stationäre, laminare, inkompressible Strömung, *Ing.-Arch.* **33**, 173–189 (1964).
7. N. Frössling, Verdunstung, Wärmeübergang und Geschwindigkeitsverteilung bei zweidimensionaler und rotationssymmetrischer Grenzschichtströmung, Engl. translation NACA TM 1432 (1958).
8. R. Hilpert, Wärmeabgabe von geheizten Drähten und Rohren im Luftstrom, *Forsch. Geb. IngWes.* **4**, 215–224 (1933).
9. E. Achenbach, Distribution of local pressure and skin friction around a circular cylinder in cross-flow up to $Re = 5 \times 10^6$, *J. Fluid Mech.* **34**, 625–639 (1968).
10. E. Achenbach and E. Heinecke, Vortex shedding from smooth and rough circular cylinders in cross flow, *J. Fluid Mech.* To be published.
11. E. Achenbach, Experimentelle Bestimmung der Impulsverlustdicke beim querangeströmten Kreiszylinder, *Wärme- und Stoffübertragung* **4**, 18–24 (1971).
12. A. Roshko, Experiments on the flow past a circular cylinder at very high Reynolds number, *J. Fluid Mech.* **10**, 345–356 (1961).
13. E. Achenbach, Heat transfer from smooth and rough surfaced circular cylinders in a cross flow, Heat Transfer Conference, Tokyo (10) FC 5 (1974).
14. H. J. Allen and W. G. Vincenti, Wall interference in a two-dimensional-flow wind tunnel with consideration of the effect of compressibility, Nat. Adv. Comm. Aero. Wash. Rep. 782 (1944).

TRANSFERT DE CHALEUR LOCAL ET GLOBAL SUR UN CYLINDRE CIRCULAIRE LISSE EN ATTAQUE TRANSVERSALE AUX NOMBRES DE REYNOLDS ELEVES

Résumé—Le transfert de chaleur local et global sur un cylindre circulaire lisse dans un écoulement d'air transversal a été mesuré dans le domaine de nombres de Reynolds $3.10^4 < Re < 4.10^6$. L'interaction entre l'écoulement et le transfert de chaleur est étudiée. En particulier, les effets de l'écoulement dans la couche limite sur le transfert thermique, tels que la transition laminaire–turbulent ou le décollement de la couche limite, sont considérés en relation avec la répartition de pression statique et le frottement pariétal.

MITTLERER UND ÖRTLICHER WÄRMEÜBERGANG BEIM KREISZYLINDER IM KREUZSTROM BEI HOHEN REYNOLDS-ZAHLEN

Zusammenfassung—Im Bereich der Reynolds-Zahlen $3 \times 10^4 < Re < 4 \times 10^6$ wurden der örtliche und integrale Wärmeübergang an Luft beim querangeströmten Kreiszylinder experimentell bestimmt. Die Beeinflussung des Wärmeübergangs durch die Strömungsvorgänge, insbesondere in der Grenzschicht des Kreiszylinders, wie z. B. durch Grenzschichtumschlag oder Strömungsablösung, wurde untersucht. Die Ergebnisse des lokalen Wärmeübergangs werden anhand der experimentellen örtlichen Druck- und Schubspannungsverteilung erläutert.

СУММАРНЫЙ И ЛОКАЛЬНЫЙ ПЕРЕНОС ТЕПЛА ОТ ГЛАДКОГО КРУГЛОГО ЦИЛИНДРА В ПОПЕРЕЧНОМ ПОТОКЕ ПРИ ВЫСОКИХ ЗНАЧЕНИЯХ ЧИСЛА РЕЙНОЛЬДСА

Аннотация — Измерялся суммарный и локальный перенос тепла при поперечном обтекании воздухом гладкого круглого цилиндра в диапазоне значений числа Рейнольдса $3 \times 10^4 < Re < 4 \times 10^6$. Обсуждается взаимосвязь между потоком воздуха и переносом тепла. В частности, зависимость процесса переноса тепла от таких эффектов пограничного слоя, как переход от ламинарного течения к турбулентному или срыв пограничного слоя, рассматривается совместно с распределением локального статистического давления и поверхностного трения.